Wang, H., Li, P. & Wang, J. (2021) Shape optimization and buckling analysis of novel two-way aluminum alloy latticed shells. Journal of Building Engineering. 36, 102100.

Shape optimization and buckling analysis of novel two-way aluminum alloy latticed shells

Hao Wang[a], Pengcheng Li[b,c*], Jie Wang[d]

a. School of Civil Engineering, Shandong Jianzhu University, Jinan, Shandong, China
b. Key Laboratory of New Technology for Construction of Cities in Mountain Area (Chongqing University), Ministry of Education, Chongqing, China
c. School of Civil Engineering, Chongqing University, Chongqing, China
d. Department of Architecture and Civil Engineering, University of Bath, UK

Abstract

The circumferential profile of cylinder, as a classic shape, has been widely adopted in single-layer latticed shells. Previous research into these structures primarily concentrated on their buckling behavior. In this work, a novel two-way aluminum alloy cable-stiffened single-layer latticed shell is proposed to explore a shape optimization procedure of such structure. In addition, the buckling behavior of the optimized structures and classic cylindrical latticed shells are examined and compared. The optimization procedure adopts a linear algorithm, in which the structural strain energy is selected to be the optimization objective. Buckling analyses are also performed to compare the buckling behavior of this novel latticed shell with classic cylindrical and optimized shapes. The comparisons show that the load-carrying capacities are clearly enhanced by optimizing the shell shapes. The results presented in this article are anticipated to aid engineers in the design of two-way aluminum alloy latticed shells with an optimal shape.

Keywords: Aluminum alloys, buckling analysis, latticed shells, prestressing, shape optimization.

1. Introduction

In construction of lightweight structures, prestressing technology has been widely adopted [1-4] owing to its ability to significantly enhance the stiffness and load-carrying capacity of structures. A cable-stiffened single-layer latticed shell is a novel prestressed structural system, which is formed by the combination of ordinary latticed shells and pre-tensioned cables [5]. The prestressing technology makes it possible to adopt quadrangular grids in single-layer latticed shells; and the pre-tensioned cables can also improve stability behavior. A large number of studies, ssuch as those focus on buckling load estimation [6-8], stability behavior evaluation [9-13], geometric imperfection investigation [14],

* Corresponding author: Pengcheng Li, lipengcheng@cqu.edu.cn

and seismic responses [15-18] have been conducted ever since the single-layer latticed shell was proposed. Practical applications of cable-stiffened single-layer latticed shells can be also found worldwide [19, 20] (Fig. 1).

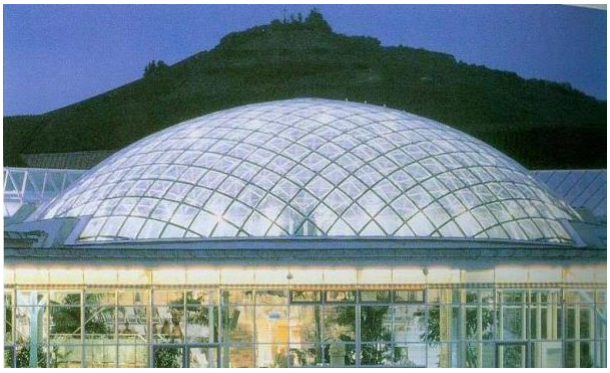

(a) Neckarsulm dome [19]

(b) Kumagaya dome [20]

Fig. 1 Practical applications of cable-stiffened latticed shells

It must be noted that previously the primary material for cable-stiffened single-layer latticed shells was steel. Compared to steels, aluminum alloys possess lighter weight, and are especially suitable for large-span latticed shells because of their potential in reducing the self-weight, which is very likely to be the dominant load in large-span structures. Aluminum alloys are also well known to be non-corrosive and recyclable, and have been adopted in the construction of several large-span latticed shells (e.g. Figs 2(a) and (b)) [21]. The behavior of aluminum alloy cable-stiffened latticed shells was unclear although there have been a few studies on unstiffened aluminum alloy latticed shells [22-23].

(a) Chenshan Botanical Garden

(b) Botanical garden in Haihua Island

Fig. 2 Practical applications of aluminum alloy latticed shells [21]

Cylindrical shells, which are three-dimensional extension of arches, are typically adopted in practice. However, it remains unclear whether this shape is the optimum solution for structures under specific loads and constraint conditions. In fact, recent research on shape optimization shows that structural behavior can be improved by modifying the shell shapes [24-30], suggesting the importance of shape optimization in structural design. It should be mentioned that although the actual structural behavior is always nonlinear, majority of shape optimization methods of latticed shells are based on linear analysis. The implementation of nonlinear buckling analysis along with shape optimization is therefore essential.

Therefore, the current study performs both shape optimization and buckling analyses to investigate the behavior of novel cable-stiffened and unstiffened two-way aluminum alloy cylindrical latticed shells. It is demonstrated that the critical buckling load and load-carrying capacities of these shells can be enhanced by shape optimization based on linear algorithm. Imperfection sensitivity analyses are also carried out, showing that the novel latticed shell is imperfection-sensitive, and its influence on different aspects of structural performance is discussed.

2. Structural systems

Two structural systems, namely the unstiffened and cable-stiffened aluminum alloy latticed shells, are considered for comparison purpose in the current study. For simplification, the unstiffened and cable-stiffened latticed shells are denoted by the acronyms ‘USLS’ and ‘CSLS’, respectively.

2.1 Two-way latticed shell geometry

The compositions and configurations of the USLS and CSLS in their initial cylindrical shapes are shown in Figs 3(a) and (b) respectively. The basic units of the USLS and CSLS are quadrangular grids, and the pre-tensioned cables are set diagonally in the grids of the stiffened shell (Fig. 3(b)).

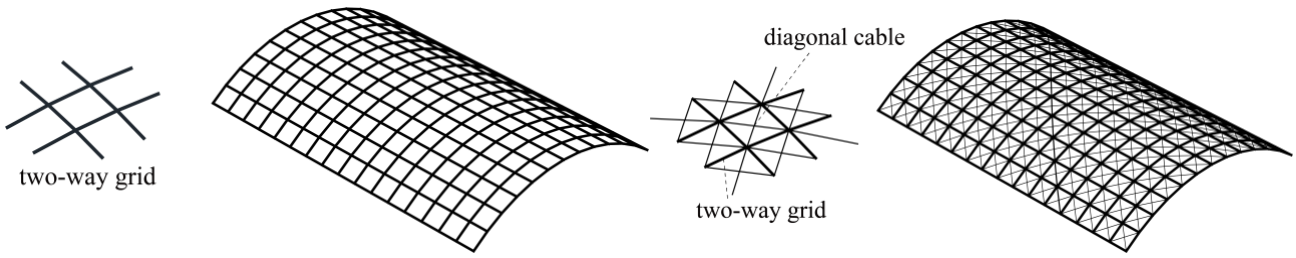

(a) USLS (b) CSLS

Fig. 3 Two-way latticed shell

Detailed dimensions of the latticed shells are given in Fig. 4, where the plan and elevation views of the shells are presented. Note that the pre-tensioned cables are not depicted in Fig. 4, as both USLS and CSLS have the same initial geometry. The span and length of the latticed shells are 24 and 36 m, respectively. The height of the highest point of the arch profile is 4 m with a rise to span ratio of 1/6. The shell is equally divided into 12 parts along the arc direction and 16 parts longitudinally (Y direction), forming 2.25 m × 2.14 m quadrangular grids.

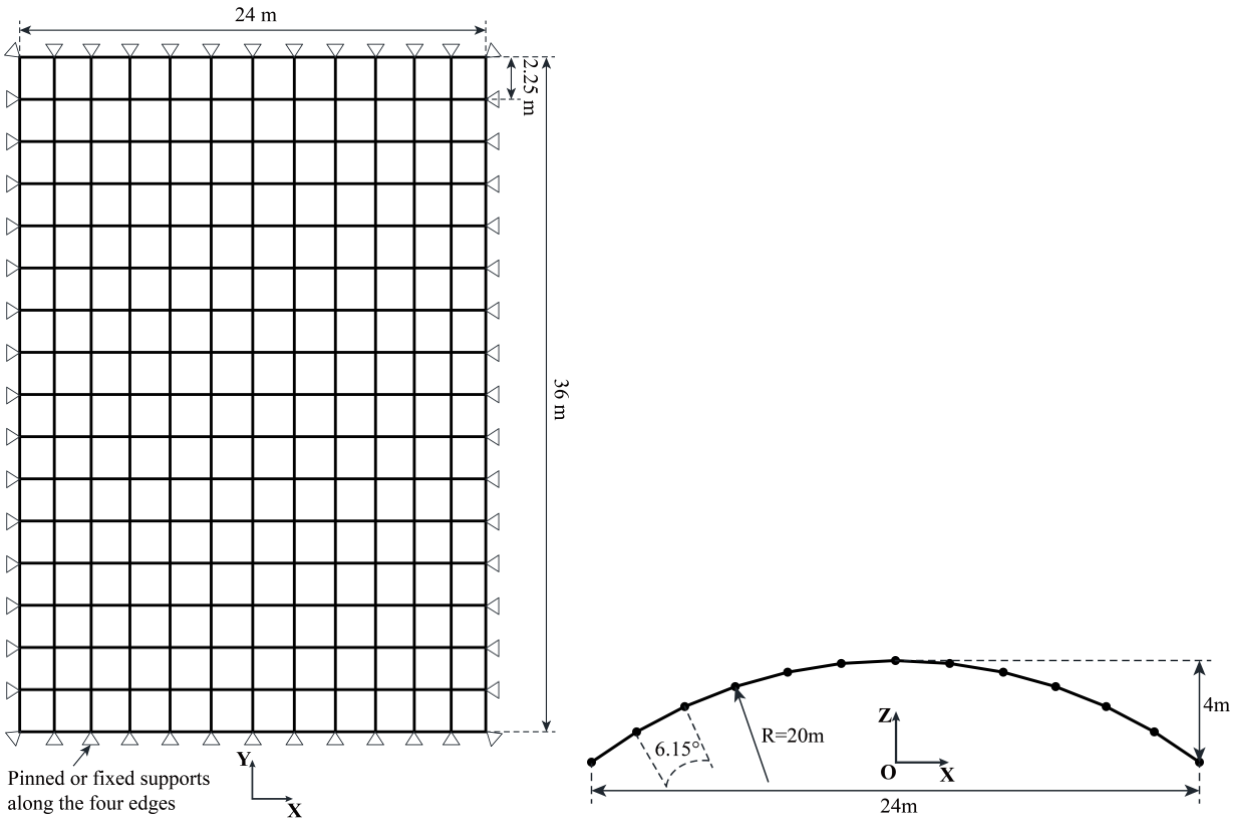

(a) Plan view (b) Elevation view

Fig. 4 Geometric parameters of cylindrical latticed shell

2.2 Materials and boundary conditions

The 6061-T6 aluminum alloy was adopted for the shell members of both the USLS and CSLS, and the spiral strand rope was adopted as the pre-tensioned cables in CSLS. The material properties of 6061-T6 aluminum was assumed to be the same as the work of Shi *et al.* [31]. In the optimization and buckling analyses, the cables were assumed to be fully elastic with a Young's modulus of 160 GPa [30]. The individual shell members are modelled with rectangular hollow cross-sections, where different cross-sections are denoted as 'section width × section height × web thickness × flange

thickness'. The members in the span and length directions are with cross-sections 250×300×10×12 and 250×250×10×10, respectively. The cross-sectional area of the cables in the CSLS varies from 50 to 300 mm^2 with an interval of 50 mm^2. The single-layer cylindrical latticed shells in practice can be supported along the four edges or the two longitudinal edges. In this work, only the case where the four edges are supported was considered, and two types of boundary conditions (i.e. pinned and fixed) were applied for comparison purpose. For simplification, the connection between two adjacent shell members was assumed to be rigid, and the connection between the pre-tensioned cable and shell member was assumed to be hinged. Since the structural optimization should be carried out under specific load conditions, a 10 kN external load was applied uniformly distributed on the grids in the optimization analyses.

3. Shape optimization method

3.1 Optimization condition and initial shape

The purpose of shape optimization of latticed shells is to identify a shape with the best structural performance (e.g. resistance, stiffness and material utilization). As an important property of a structure, the strain energy is associated with its structural performance under static loads and can provide a reference for the stiffness. The smaller the strain energy, the more efficient the structure. The minimization of strain energy was therefore chosen as the optimization objective.

Fig. 5(a) and (b) presents the initial shapes of the USLS and CSLS, respectively, where the grid points were set to be the same. The optimization variables were the z-coordinates of the grid points with a feasible region defined. In order to maintain the rise to span ratio less than 1/4, the maximum and minimum z-coordinates of grid points are limited to 6 and −6 m, respectively; the feasible region is therefore defined as:

$$\begin{cases} z_{\min} = -6 \text{ m} \\ z_{\max} = 6 \text{m} \end{cases} \tag{1}$$

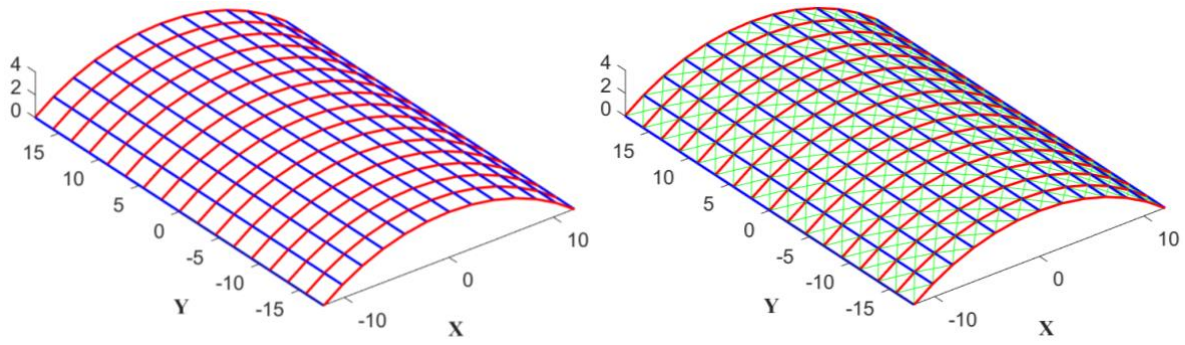

(a) USLS (b) CSLS

Fig. 5 Initial shapes of latticed shells

3.2 Sensitivity analysis of strain energy

In linear finite element analysis of a structure, it is well known the classic expression Eq. (2).

$$\mathbf{KU} = \mathbf{F} \tag{2}$$

where **K** is the stiffness matrix, **U** is the nodal displacement vector, and **F** is a nodal load vector given by the design load. The strain energy of the structure C can be calculated by Eq. (3).

$$C = \frac{1}{2}\mathbf{F}^T\mathbf{U} \tag{3}$$

The optimization analysis requires sensitivity analyses of the strain energy based on Eq. (3). By differentiating Eqs (2) and (3) with respect to the z-coordinate of grid point *i*, the following equations can be obtained.

$$\frac{\partial \mathbf{K}}{\partial z_i}\mathbf{U} + \mathbf{K}\frac{\partial \mathbf{U}}{\partial z_i} = \frac{\partial \mathbf{F}}{\partial z_i} \tag{4}$$

$$\frac{\partial C}{\partial z_i} = \frac{1}{2}\left(\mathbf{F}^T\frac{\partial \mathbf{U}}{\partial z_i} + \frac{\partial \mathbf{F}^T}{\partial z_i}\mathbf{U}\right) \tag{5}$$

Assuming that the nodal load vector does not change, Eq. (4) can be substituted into Eq. (5), and a rearrangement will give the derivative of the strain energy C with respect to z_i as:

$$\frac{\partial C}{\partial z_i} = \frac{1}{2}\mathbf{U}^T\frac{\partial \mathbf{K}}{\partial z_i}\mathbf{U} \tag{6}$$

3.3 Optimization equation

The optimization equation for minimum strain energy can be formulated as follows:

$$\min_{z\in R^n} C(\mathbf{Z}) \quad \text{subject to } h_i(\mathbf{Z}) \geq 0 \tag{7}$$

where $C(\mathbf{Z})$ denotes the strain energy, and $\mathbf{Z}$ denotes the z-coordinates of grid points; $h_i(\mathbf{Z})$ expresses the constraint function:

$$h(\mathbf{Z}): \begin{cases} h_i^{\max}(z_i) = z_i^{\max} - z_i \\ h_i^{\min}(z_i) = z_i - z_i^{\min} \end{cases} \quad i \in \tau, z_i \in \mathbf{Z} \tag{8}$$

where $z_i^{\max}$ and $z_i^{\min}$ are the maximum and minimum z-coordinates of point i, respectively. By using the interior-point method, the constraint optimization problem can be rewritten as follows:

$$\min_{z\in R^n} f(\mathbf{Z}, r_k) = C(\mathbf{Z}) - r_k \sum_{i\in\tau} (\ln h_i^{\min}(z_i) + \ln h_i^{\max}(z_i)) \tag{9}$$

where a positive value, r_k, is the penalty factor; it is scaled down by a positive value ($c < 1$) in steps:

$$r_k = c \cdot r_{k-1}. \tag{10}$$

The conjugate gradient method is employed to solve the optimization problem; the gradient of Eq. (9) can be written as follows:

$$\nabla f(\mathbf{Z}, r_k) = \nabla C(\mathbf{Z}) - r_k \nabla \sum_{i\in\tau} \left(\ln h_i^{\min}(z_i) + \ln h_i^{\max}(z_i)\right). \tag{11}$$

where $\nabla C(\mathbf{Z})$ denotes the gradient of strain energy with respect to the z-coordinates of grid points. The ith element in $\nabla C(\mathbf{Z})$ is $\partial C/\partial z_i$, as can be derived according to the sensitivity analysis in Section 3.2. The derivative of the barrier function with respect to z_i can be expressed as

$$\frac{\partial \sum_{i\in\tau} (\ln h_i^{\min}(z_i) + \ln h_i^{\max}(z_i))}{\partial z_i} = \sum_{i\in\tau} \left(\frac{1}{z_i - z_i^{\min}} - \frac{1}{z_i^{\max} - z_i} \right). \tag{12}$$

3.4 Optimization process

According to the shape optimization equation and sensitivity analysis for strain energy, the process of shape optimization can be illustrated by a double-iteration algorithm, as follows.

Step 1: Set the structural parameters and optimization conditions; assign the initial shape and proceed

to **Loop I**.

Loop I:

Step 2: Establish the optimization equation as Eq. (9) according to the constraint function and penalty factor and proceed to **Loop II**.

Loop II:

Step 3: Perform the sensitivity analysis based on Eq. (6); obtain the gradient of the strain energy.

Step 4: Calculate the gradient of Eq. (9).

Step 5: Determine the step length according to unidimensional search algorithm, i.e., golden section method; update the shape.

Step 6: If the convergence conditions are satisfied, end **Loop II**, otherwise return to Step 3.

End Loop II.

Step 7: If the optimization conditions are satisfied, end **Loop I**, otherwise scale down the penalty factor using Eq. (10) and return to step 2.

End Loop I.

Step 8: Obtain the optimal solution.

4. Optimization

The shape optimization method introduced in Section 3 was applied to a range of USLSs and CSLSs with varying cable cross-section sizes and boundary conditions (varying parameters are detailed in Section 2). The pretension in cable is considered to be high enough so that the cable does not go slack under the design load. The outcomes of the shape optimization analysis include the optimal shapes, the strain energy and critical buckling load of the structure, average and maximum z-directional displacements of the grid points, and average and maximum normal stresses of the individual shell members which were modelled with beam elements. These results are presented in this section to

illustrate the changes in the structural performances during optimization, and compare the structural performances between initial and optimal shapes for the different cable cross-sectional areas and the two bourdary conditions.

4.1 Optimal shapes

Figs 6 and 7 present the optimized shapes of the USLS and CSLS with different cable cross-section sizes with pinned and fixed boundary conditions, respectively. Compared to the height of the initial shape, the height of grid points after optimization are generally larger. Recalling the relationship between the structural rigidity and the strain energy, it is reasonable for the optimal shapes of USLS and CSLS to possess higher rise to span ratios in correspondence to lower strain energy. It should be noted that the optimal shapes of CSLS with different cross-sectional areas are similar regardless of the boundary conditions. This is bacause the pre-tensioned cables improve mainly the in-plane shear rigidity of the grid, but have little effect on the out-of-plane rigidity.

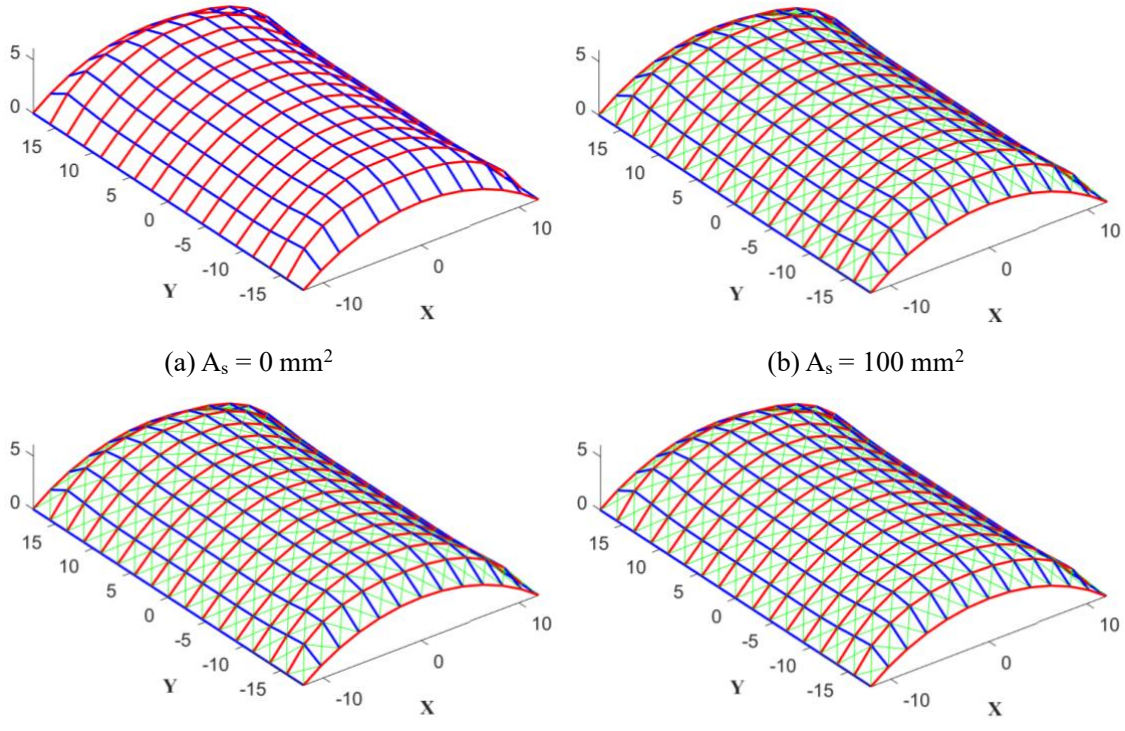

(a) A_s = 0 mm^2 (b) A_s = 100 mm^2

(c) A_s = 200 mm^2 (d) A_s = 300 mm^2

Fig. 6 Optimal shapes of USLS and CSLS with pinned supports

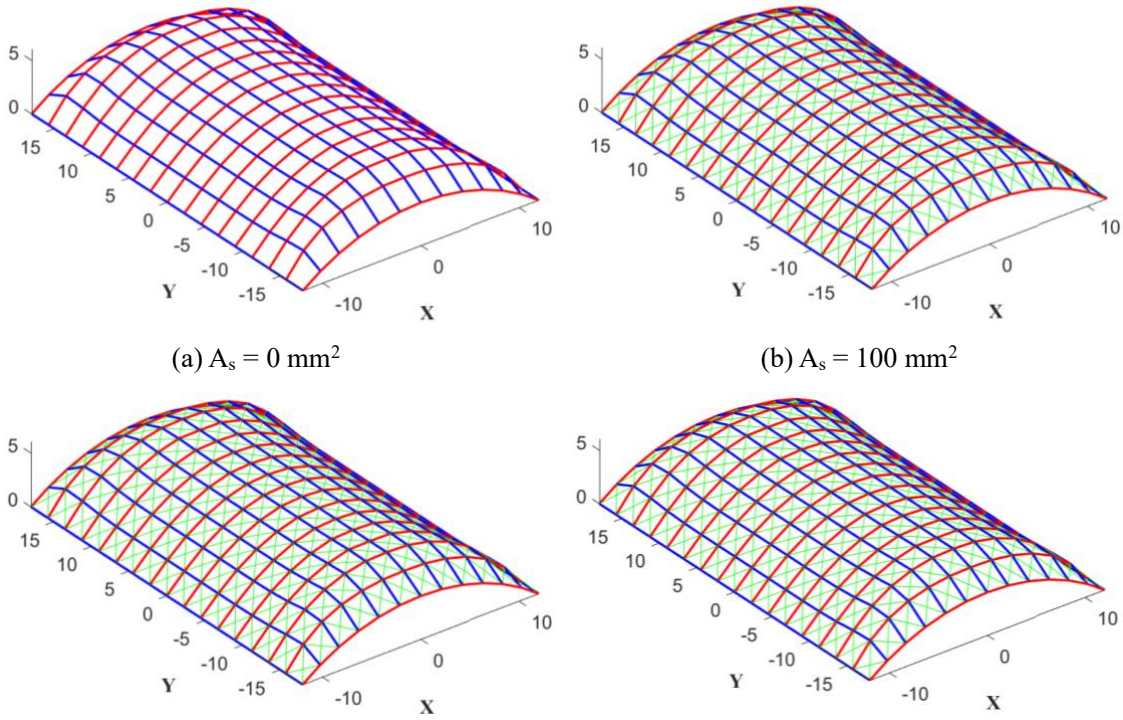

(a) A_s = 0 mm^2 (b) A_s = 100 mm^2

(c) A_s = 200 mm^2 (d) A_s = 300 mm^2

Fig. 7 Optimal shapes of USLS and CSLS with fixed supports

4.2 Structural performance during optimization

4.2.1 Latticed shells with pinned supports

The changes in strain energy and other aspects of structural performance during optimization are presented in Fig. 8. The numbers in the legends denote the cross-sectional areas of the cables; the USLSs are represented by '0'. In Fig. 8(a), it can be observed that for all the shells the strain energy significantly decreases in the first few steps and thereafter gradually converges to the minimum value. Figs 8(c)-(f) indicate that the displacement and normal stresses decrease after the optimization. The critical buckling resistance, however, as shown in Fig. 8(b) is increased as a result of optimization for all the cases. It is further observed that apart from strain energy, the other aspects of structural performance do not vary monotonously as the number of iterations increases. Overall, the optimization results of pin-supported latticed shells indicate that the strain energy in each shell has been successfully minimized, and the other aspects of structural performance have been effectively improved.

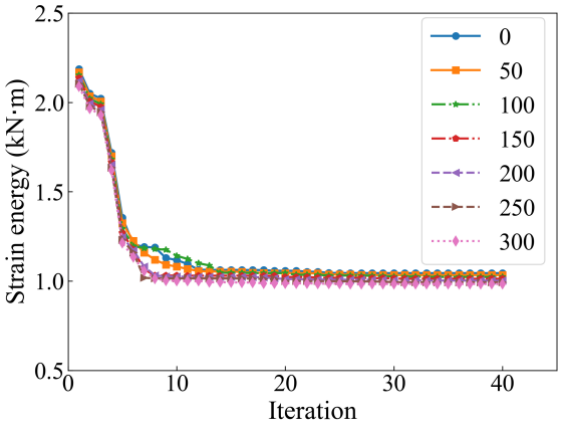

(a) Strain energy during optimization

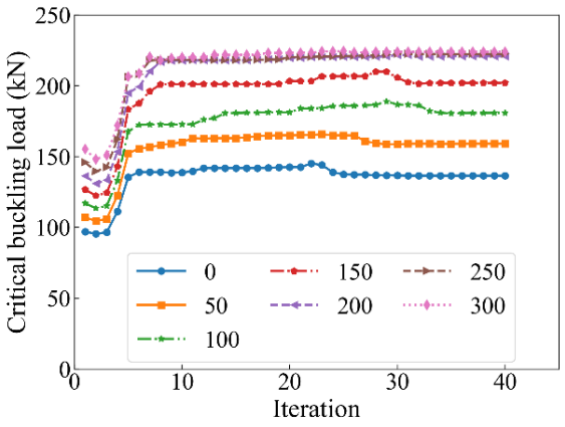

(b) Critical buckling load during optimization

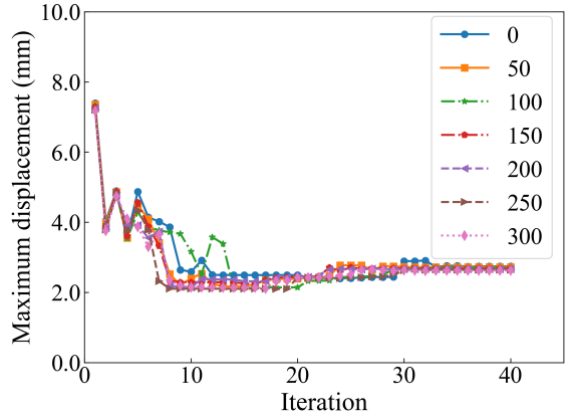

(c) Maximum displacement during optimization

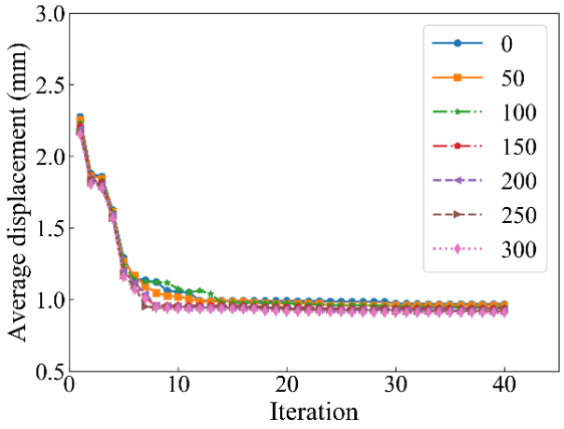

(d) Average displacement during optimization

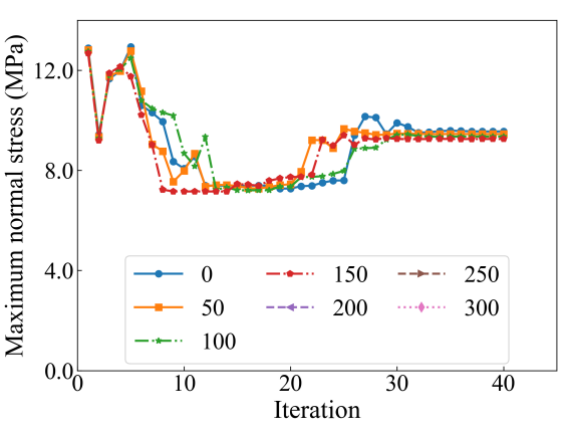

(e) Maximum normal stress during optimization

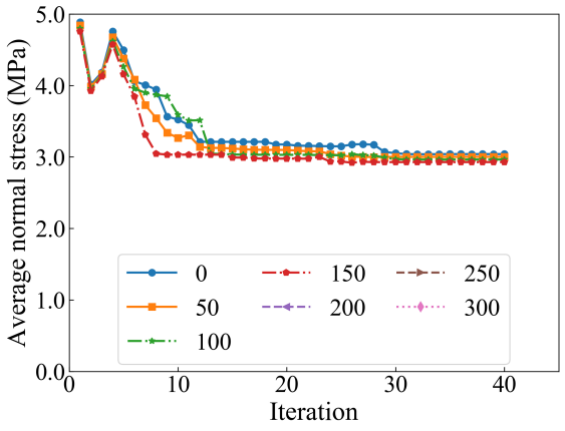

(f) Average normal stress during optimization

Fig. 8 Structural performance of USLS and CSLS with pinned supports during optimization

4.2.2 Latticed shells with fixed supports

Fig. 9 presents the changes in the structural performance of USLS and CSLS with fixed supports during optimization. Very similar outcomes as for pinned supported shells have been achieved in fixed

supported shells, where the strain energy significantly decreased and reached a minimum value during the optimization (Fig. 9(a)), and the other aspects of structural performance were improved after optimization (Figs 9(b)-(f)). It should be noted that in the first few steps the strain energy decreased rapidly, whereas the maximum and average normal stresses evidently increased. This indicates that the shape optimization method, aiming at obtaining the minimum strain energy, does not necessarily optimize the other aspects of structural performance.

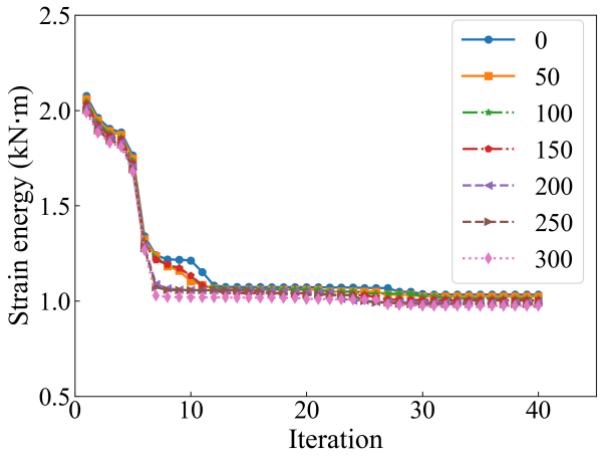

(a) Strain energy during optimization

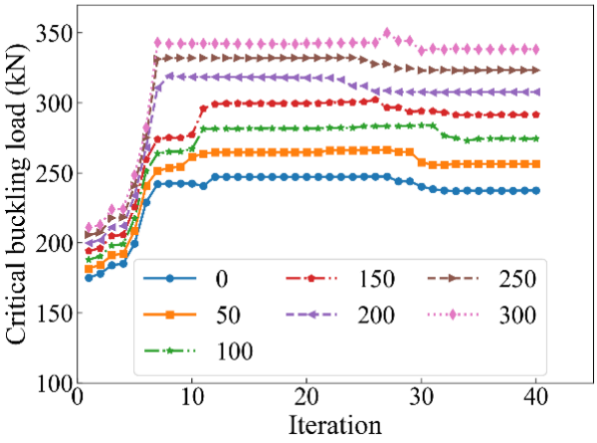

(b) Critical buckling load during optimization

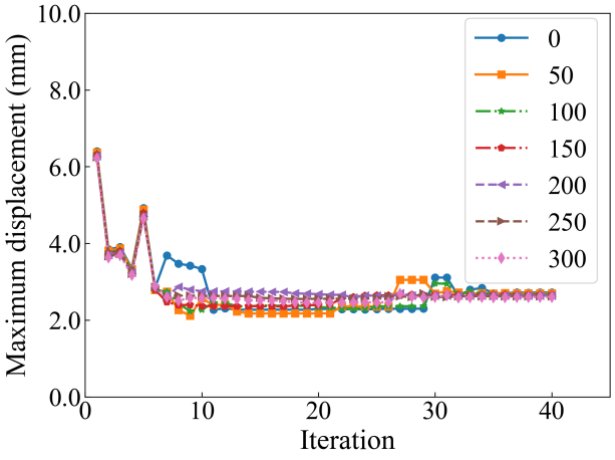

(c) Maximum displacement during optimization

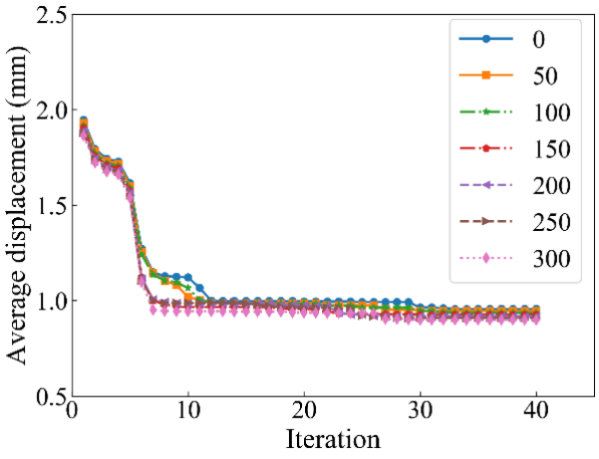

(d) Average displacement during optimization

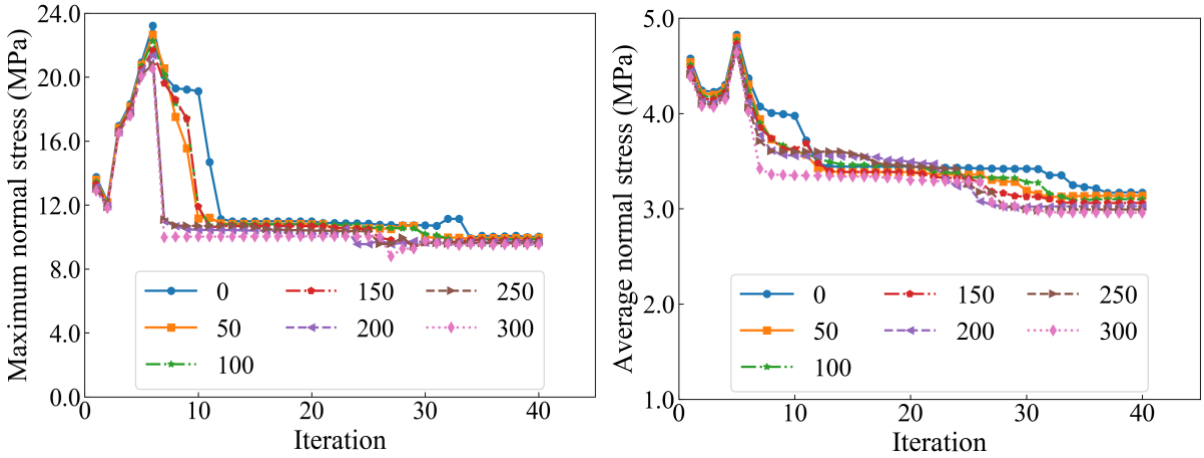

(e) Maximum normal stress during optimization (f) Average normal stress during optimization

Fig. 9 Structural performance of USLS and CSLS with fixed supports during optimization

As mentioned above, the strain energy can be used as a benchmark for estimating the structural rigidity of USLS and CSLS. The smaller the strain energy, the higher rigidity the structure possesses. Therefore, the normal stress of members and the displacement of grid points decrease as the rigidity increases in the optimization process.

4.3 Comparison of results before and after optimization

4.3.1 Pinned supported latticed shells

The structural performances of the initial and optimal shapes for pinned supported shells are summarized in Fig. 10, where the percentage changes in the strain energy, buckling load, maximum and average displacements, and maximum and average normal stresses before and after optimization are given as bar charts. In general, the improvements in displacements and normal stresses for shells are very similar for the various cable cross-sections considered (~63% in maximum displacement, ~57% in average displacement, ~27% in maximum normal stress and ~38% in average normal stress). However, the optimized shapes present various buckling resistance improvements depending on their cable cross-sectional areas, where the shell with $A_s = 200$ mm^2 presents the highest buckling resistance improvement (61.9%) whereas the optimized USLS shell ($A_s = 0$ mm^2) has only 40% increase in its buckling resistance.

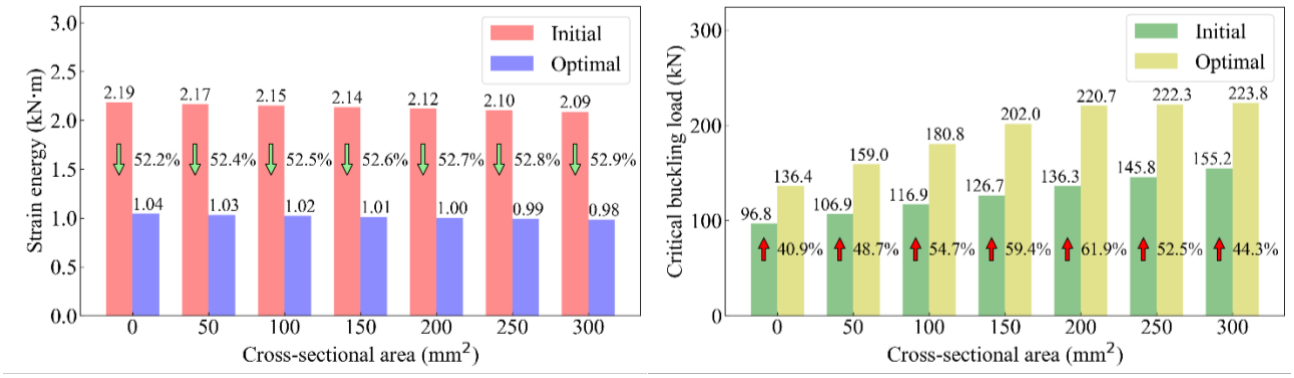

(a) Strain energy

(b) Critical buckling load

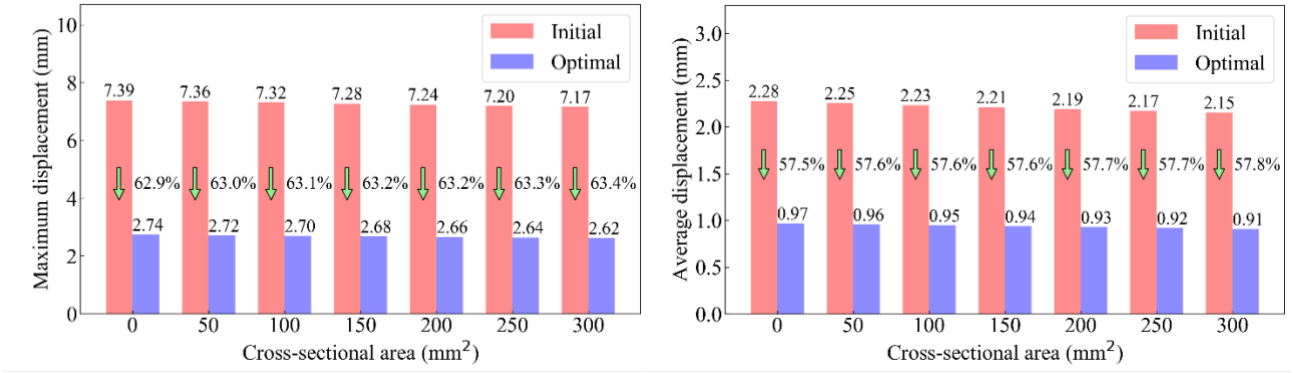

(c) Maximum displacement

(d) Average displacement

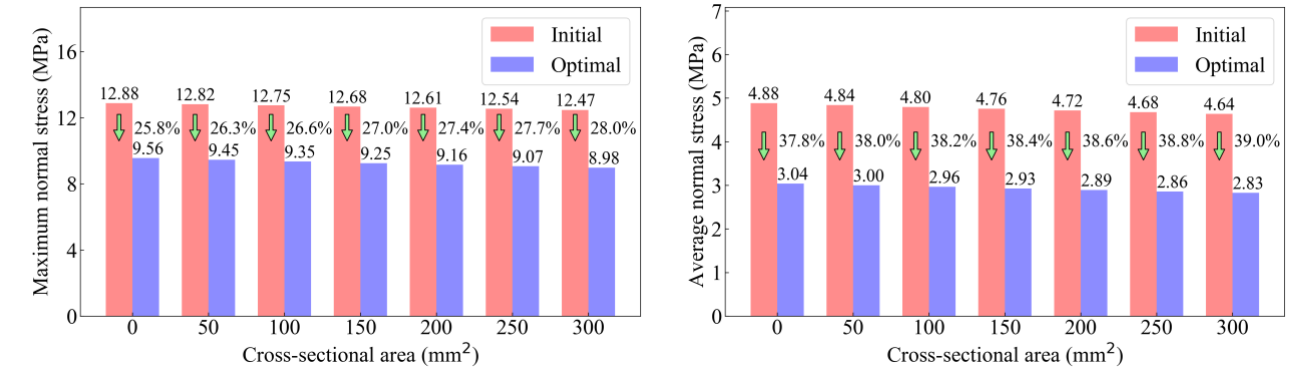

(e) Maximum normal stress

(f) Average normal stress

Fig. 10 Comparison of structural performances of pinned supported USLS and CSLS in initial and optimized shapes

4.3.2 Fixed supported latticed shells

Fig. 11 compares the structural performances of the initial and optimal shapes of USLS and CSLS with fixed supports. It shows that the improvements in strain energy, displacement and normal stress level brought by optimization (Fig. 11(a) and (c)-(f)) are similar to those in the pinned supported cases (Fig. 10(a) and (c)-(f)), and do not vary significantly with varying cable cross-sectional areas. However, the

buckling load enhancement brought by optimization is constantly increasing as the cable cross-sectional area increases (Fig. 11(b)), which is different from that in the pinned supported case (Fig. 10(b)). The shape optimization can increase the critical buckling load by 60.2% at A_s = 300 mm^2.

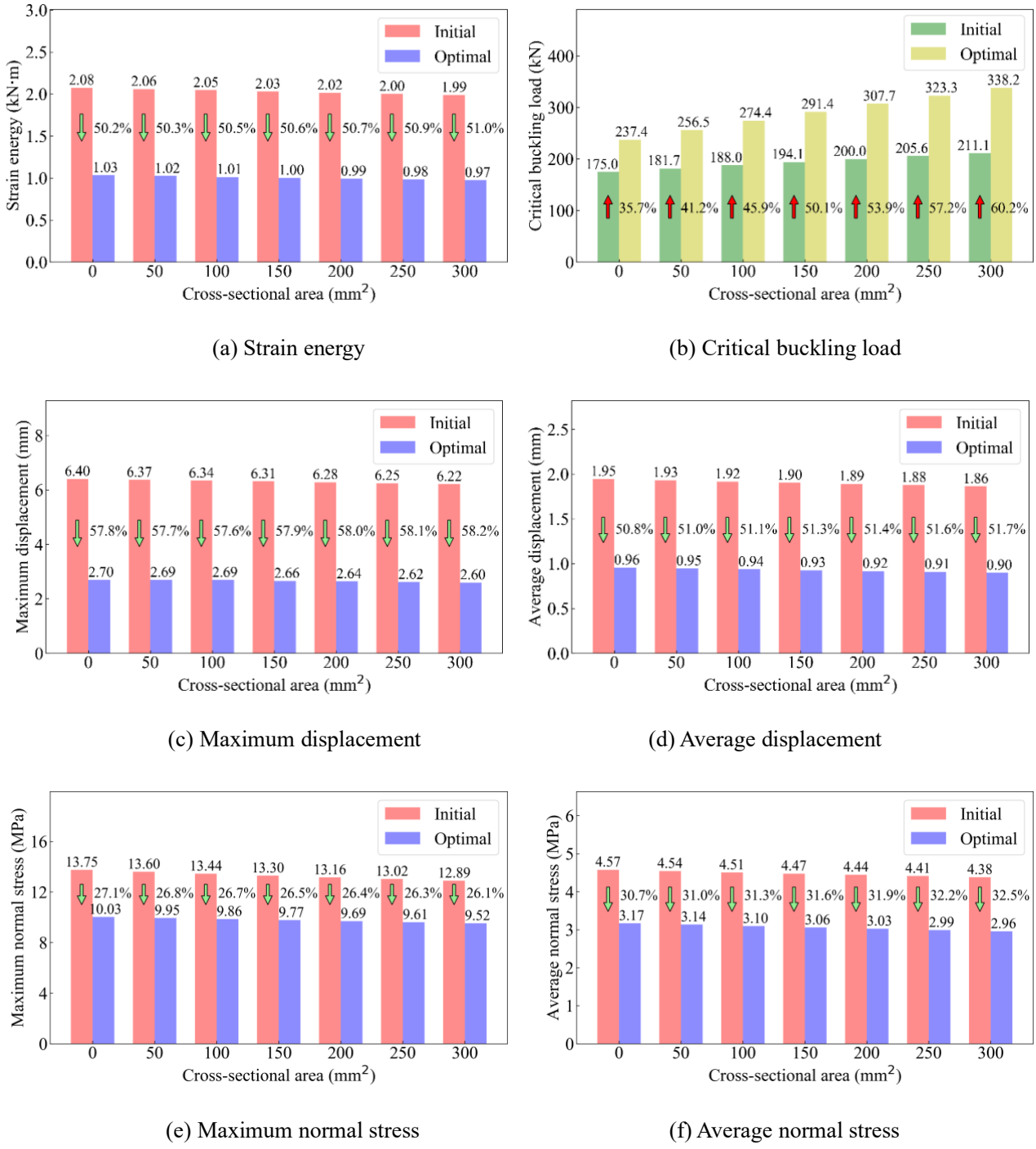

(a) Strain energy

(b) Critical buckling load

(c) Maximum displacement

(d) Average displacement

(e) Maximum normal stress

(f) Average normal stress

Fig. 11 Comparison of structural performances of fixed supported USLS and CSLS in initial and optimized shapes

4.3.3 Degree of variation of structural performance

Fig. 12 summarizes again the variation of structural performance with the cross-sectional area of the cable and boundary condition, with the vertical axis Δ being the percentage increment after the shape optimization. It shows that the percentage increments of strain energy, displacements and normal stress levels are almost invariant with the changing cable cross-sectional area, whereas the improvement in critical buckling load due to optimization display a clear dependence on the size of the cable, and the variations are different in the pinned and fixed supported shells - the buckling load is optimized at A_s = 200 mm^2 for pinned supported shells (Fig.12(a)) whereas the buckling constantly increases with the cable size in fixed supported shells (Fig. 12(b)).

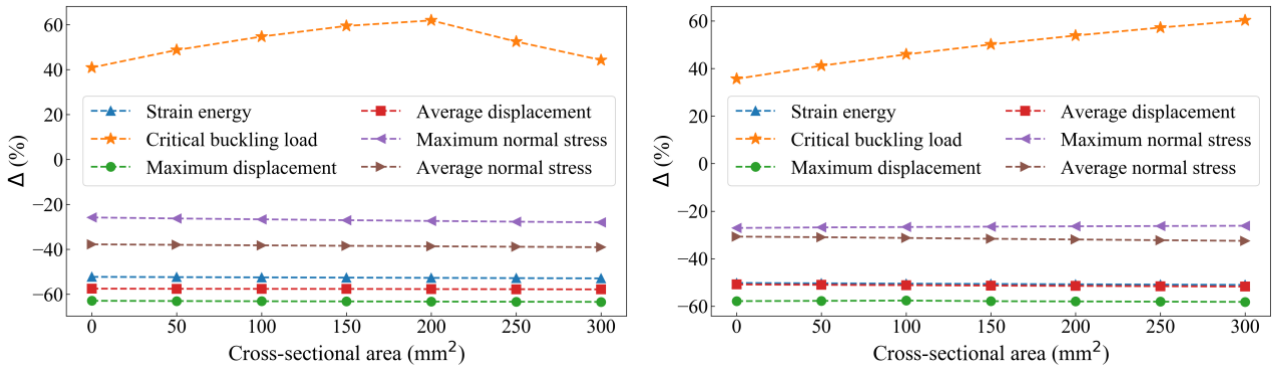

(a) Latticed shells with pinned supports (b) Latticed shells with fixed supports

Fig. 12 Variation rates of structural performance

The above results indicate that the proposed shape optimization can effectively minimize the strain energy of the shell and can significantly improve the loading capacity and stiffness of the structure. It should be noted that the shape optimization method is based on linear finite element analysis, and the structural performances investigated in the example are also calculated from their linear responses. However, studies have shown that geometric and material nonlinearities can significantly influence the structural performance of latticed shells [11, 14]. It is therefore necessary to investigate the nonlinear performance of latticed shells in their optimized shapes. In the following section, a series of nonlinear analyses performed on latticed shells are presented, and the nonlinear performances of the initial and optimal shapes are discussed.

5. Buckling analyses

To investigate the stability performance of CSLS and USLS in their initial and optimal shapes, a series of nonlinear buckling analyses were carried out employing the commercial software ANSYS. In the numerical models, the aluminum alloy members and cables of the latticed shells were represented by beam elements and tension-only link elements, respectively. Each aluminum alloy member was meshed with six beam elements and each cable was meshed as a single link element. Prior to the nonlinear analyses, corresponding linear eigenvalue analyses were conducted to obtain the critical buckling modes to be used as initial geometric imperfection form in the nonlinear analyses.

5.1 Linear eigenvalue analysis

Fig. 13 presents the critical buckling modes of USLS and CSLS with initial and optimal shapes (denoted as 'Ini' and 'Opt' respectively) under fixed and pinned support conditions (denoted as 'fix' and 'pin' respectively). Note that the cross-sectional areas of the cables in the CSLS as shown in Fig.(13e)-13(h) are 300 mm^2. It can be observed that the critical buckling mode of USLS remains the same before and after shape optimization for both pinned and fixed support conditions, whereas the eigenmode of pinned supported CSLS changed from two half sine waves to three half sine waves by shape optimization for pinned support cases.

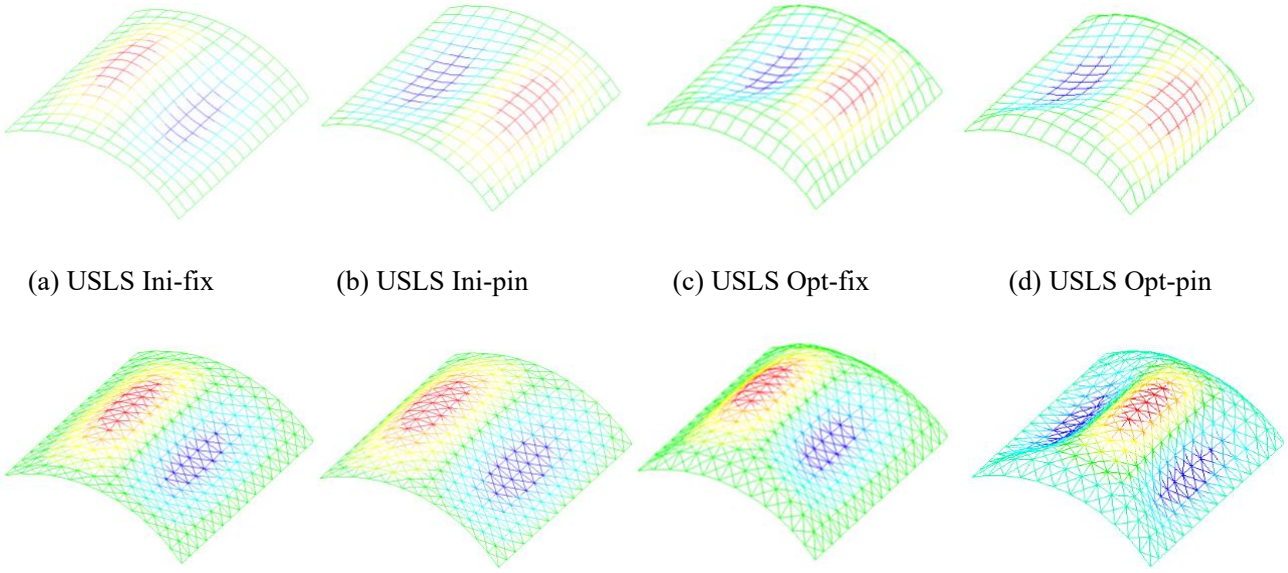

(a) USLS Ini-fix (b) USLS Ini-pin (c) USLS Opt-fix (d) USLS Opt-pin

(e) CSLS Ini-fix (f) CSLS Ini-pin (g) CSLS Opt-fix (h) CSLS Opt-pin

Fig. 13 Critical buckling modes

5.2 Governing geometric imperfection form

For single-layer latticed shells, it has been proved that the governing geometric imperfection in nonlinear buckling analysis can be symmetric or anti-symmetric [11]. Similarly, it is essential to determine the governing imperfection form in USLS and CSLS. This issue was resolved by the procedure below:

(1) Conduct linear buckling analysis (eigenvalue analysis) to obtain the eigenmodes that correspond to the first symmetric and the first anti-symmetric buckling shapes.

(2) Perform nonlinear buckling analyses in which the symmetric and anti-symmetric buckling modes obtained from the linear buckling analysis are separately incorporated as the imperfection forms.

(3) Compare the load carrying capacities obtained from the nonlinear buckling analyses and the imperfection mode that generates lower load carrying capacity is considered to be the governing imperfection form.

Fig. 14 shows the load versus displacement curves of optimal CSLS with symmetric and anti-symmetric imperfection distributions when the boundary conditions are pinned and fixed. It should be noted that the cross-sectional area of the cables in CSLS of Fig. 14 is 300 mm^2, and the imperfection magnitude is L/300 (L is the span of CSLS). It can be seen clearly that the anti-symmetric imperfection distribution corresponds to a lower load bearing capacity, implying that this anti-symmetric shape should be taken as the governing imperfection form in nonlinear buckling analysis. For the nonlinear analyses in the following sections of this paper, the governing imperfection forms for all the cases are determined used the same procedure as set out herein. Note that the initial pretension in cables was set as 300 MPa in the nonlinear buckling analyses of this study to ensure that the shell members buckle prior to cable slackening.

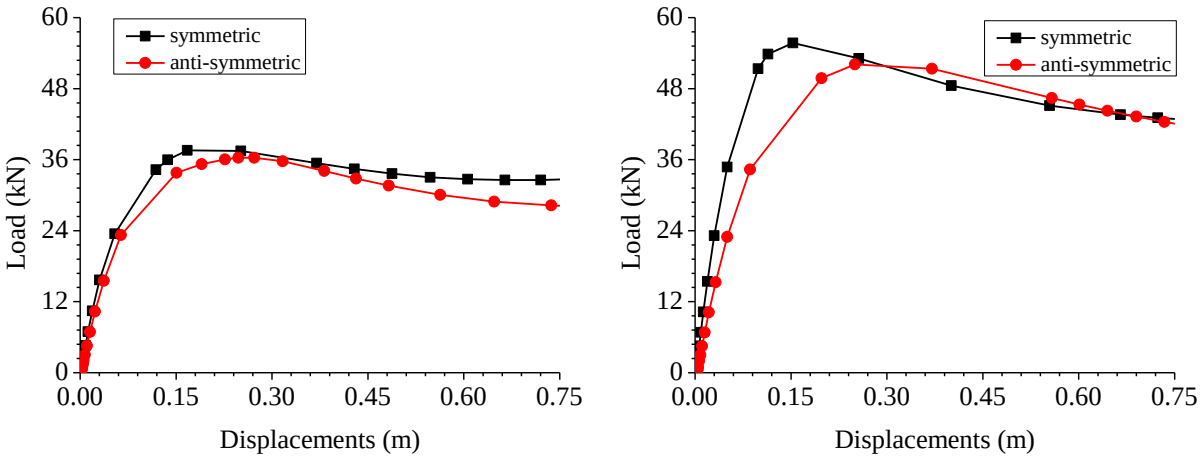

(a) Pinned supported (b) Fixed supported

Fig. 14 Load versus displacement curves of CSLS with symmetric and anti-symmetric imperfection forms (A_s = 300 mm^2)

5.3 Load-carrying capacities of latticed shells

Fig. 15 presents the load versus displacement curves of the USLS and CSLS with initial and optimal shapes under fixed and pinned support conditions. In Fig. 15, the vertical axis represents the external nodal load and the horizontal axis denotes the maximum nodal displacement in the z-direction when buckling occurs. For simplification, 'Opt-' and 'Ini-' denote results that correspond to the optimal and initial shapes of latticed shells, respectively. As shown in Fig. 15(a), the load-carrying capacity of the USLSs with the initial shape under fixed and pinned support conditions is approximately 20 kN. The load-carrying capacities corresponding to the optimal shapes increase to approximately 30 and 42 kN under pinned and fixed support conditions, respectively. In other words, shape optimization can significantly enhance the load-carrying capacities of USLSs; similar results can be also observed for CSLSs, as shown in Figs 15(b)-(g). The load-carrying capacities of CSLSs are considerably improved when the shell shape is changed from initial to optimal.

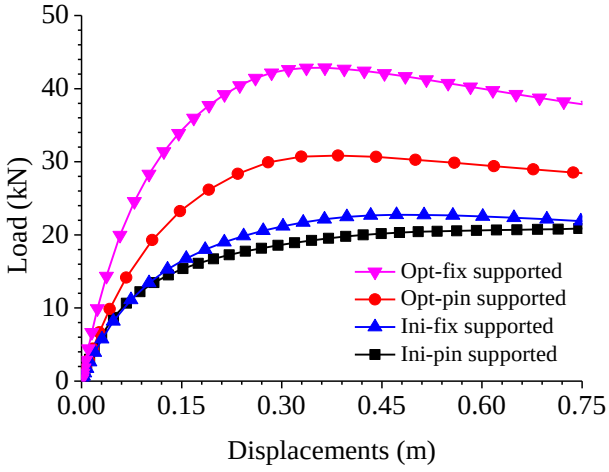

(a) $A_s = 0$

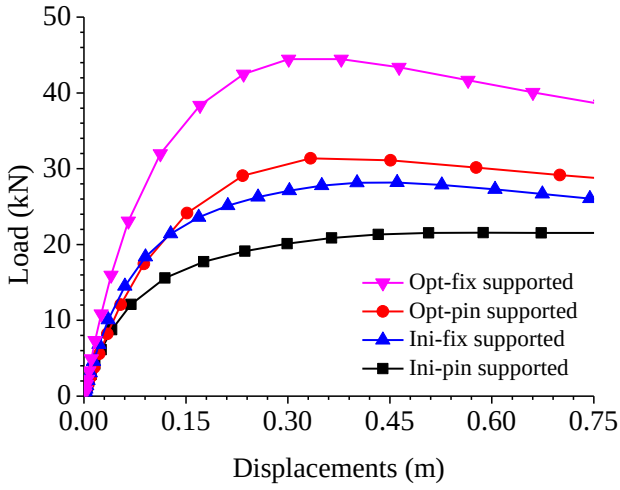

(b) $A_s = 50$ mm^2

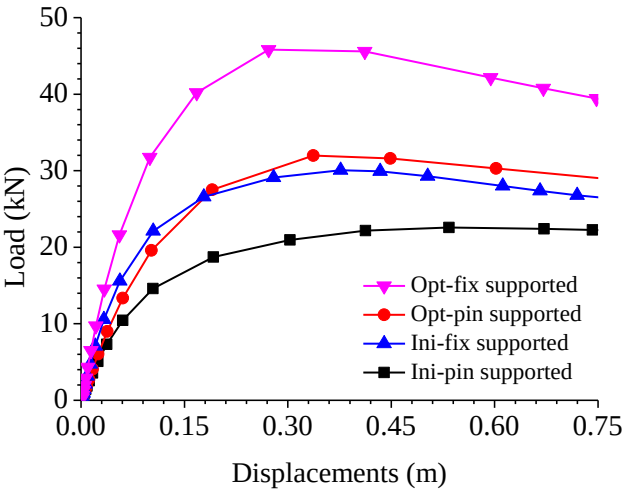

(c) $A_s = 100$ mm^2

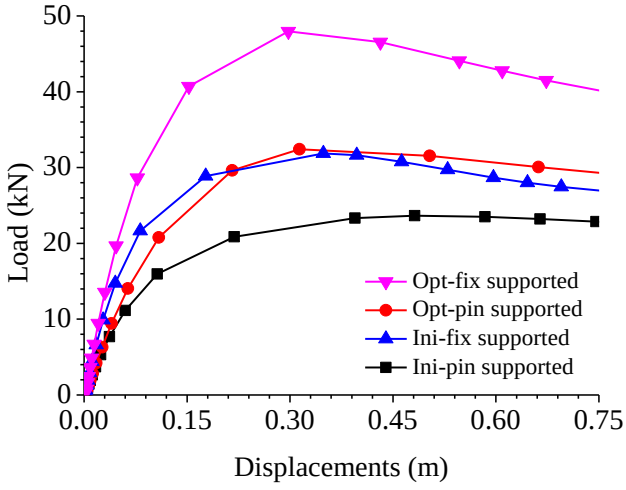

(d) $A_s = 150$ mm^2

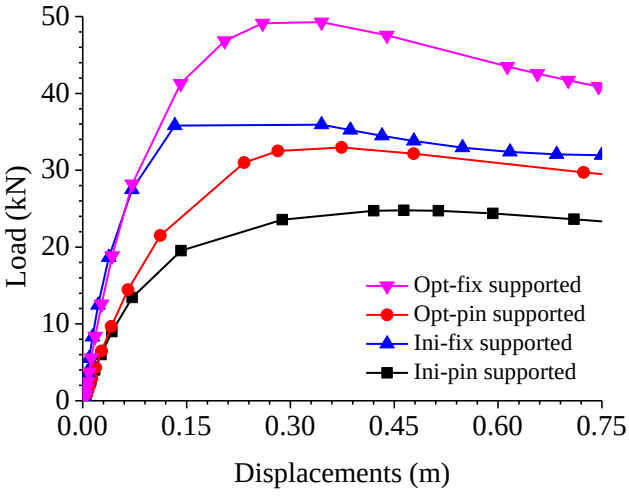

(e) $A_s = 200$ mm^2

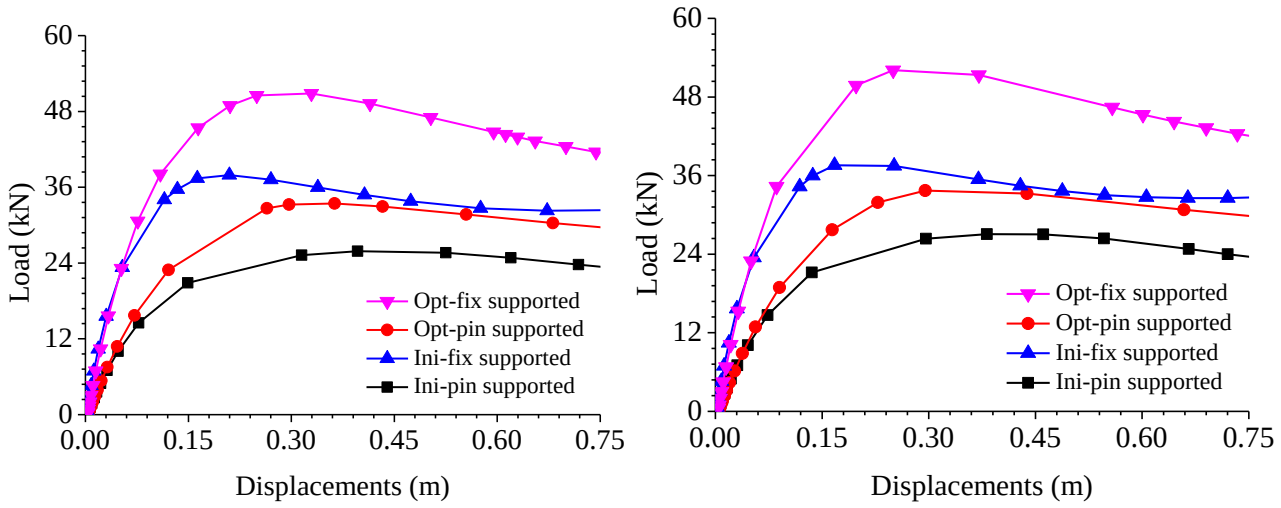

(f) A_s = 250 mm^2 (g) A_s = 300 mm^2

Fig. 15 Load versus displacement curves of latticed shells with different cable cross-sectional areas

Fig. 16 presents the load-carrying capacities of two-way single-layer latticed shells with varying cross-sectional areas and boundary conditions. It is evident that optimizing the shell shape enhances the load-carrying capacities of both unstiffened and stiffened latticed shells, especially in cases where the supports are fixed. It should also be noted that the load-carrying capacities of the CSLSs are higher than those of USLSs; this means that the introduction of pre-tensioned cables into two-way aluminum alloy latticed shells is effective in terms of improving the load-carrying capacity.

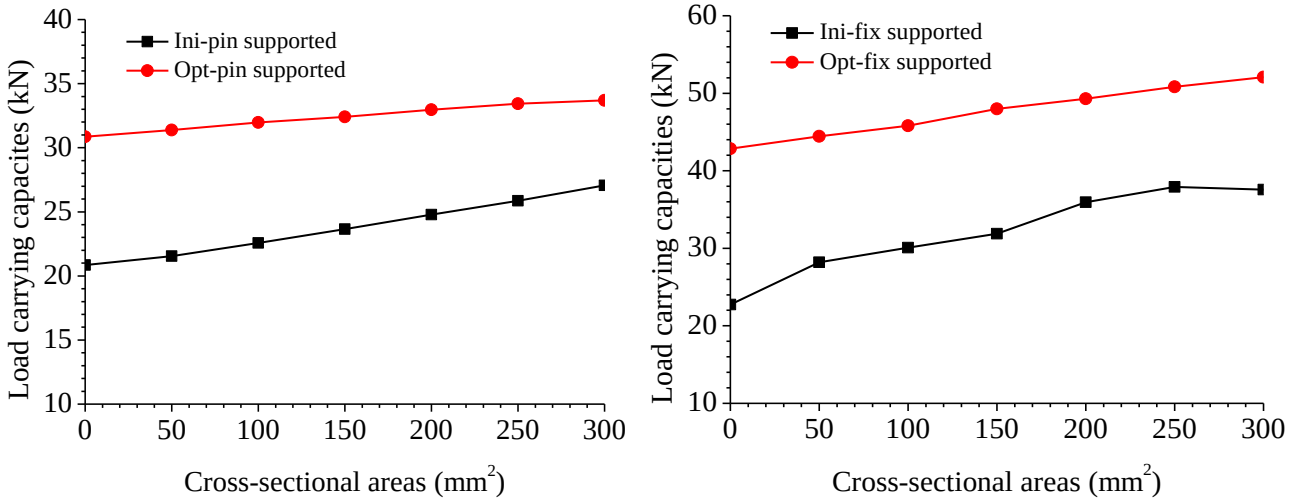

(a) Pinned supported (b) Fixed supported

Fig. 16 Variation of load-carrying capacity with cable cross-sectional area

5.4 Imperfection sensitivity study

In the discussion above, the imperfect shells were with imperfection amplitude of L/300, with L being the span of the shell. In this section, results of shells with imperfection amplitudes ranging from L/10,000 to L/100 are discussed to demonstrate the imperfection sensitivity of latticed shells before and after optimization. It should be noted that the imperfection amplitude L/10,000 represents the nearly perfect state, L/100 represents a very imperfect case, and those varying from L/2,000 to L/300 represent the cases in between.

Fig. 17 presents the load versus displacement of imperfect latticed shells in their initial and optimal shapes under different support conditions. It is clearly shown in Fig. 17 that imperfection deteriorates the resistance of structure for all the cases under consideration. When the latticed shells are not cable stiffened ($A_s = 0$; Figs 17(a)-(d)), the fixed supported shells (Figs 17(b) and (d)) are more imperfection sensitive compared to their pined counterparts (Figs 17(a) and (c)), whereas the cable stiffened latticed shells (CSLS) with $A_s = 150$ mm^2 display stronger imperfection sensitivity in the pinned support condition prior to optimization (Fig. 17(f) in comparison with Fig. 17(e)). After shape optimization, both pinned supported and fixed supported CSLS (Figs 17(g) and (h)) display similarly stronger imperfection sensitivity compared to their un-optimized states (Figs 17(e) and (f)).

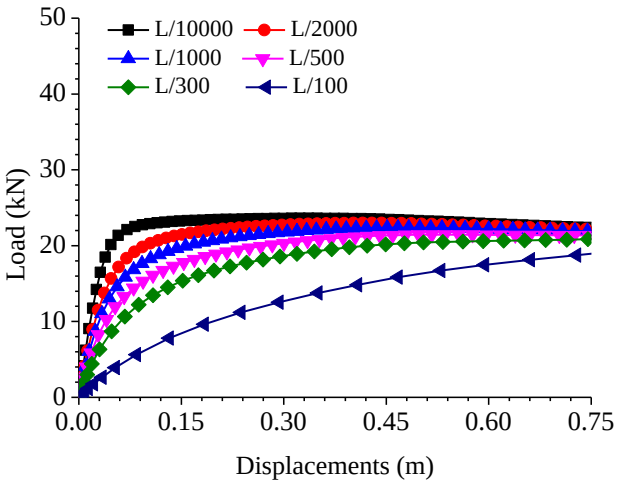

(a) Ini-pin supported when $A_s = 0$

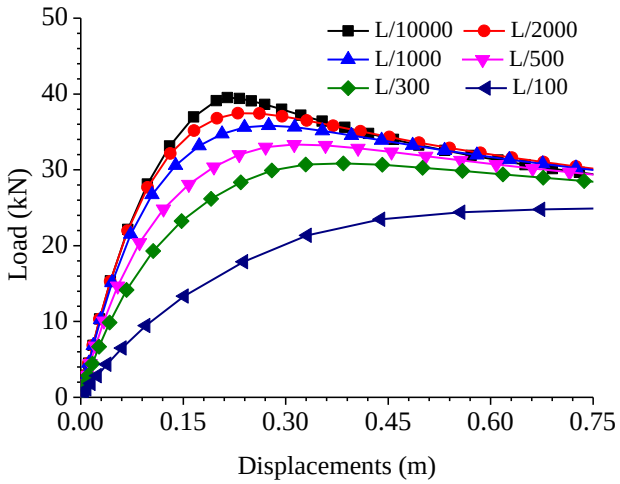

(b) Ini-fix supported when $A_s = 0$

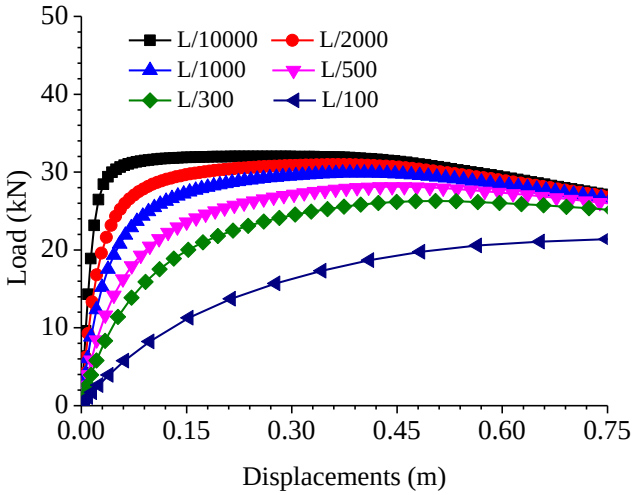

(c) Opt-pin supported when $A_s = 0$

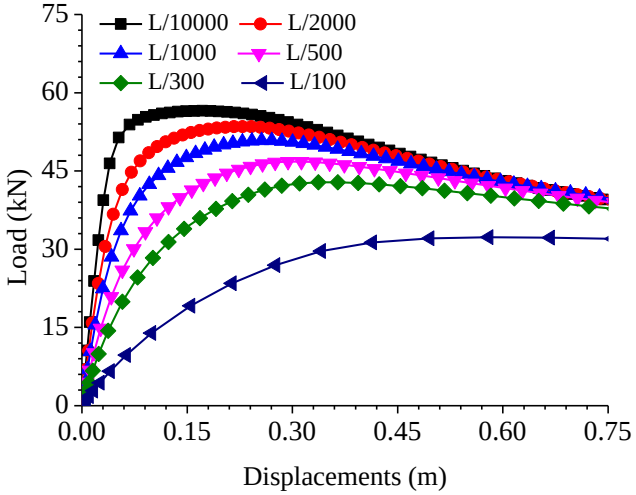

(d) Opt-fix supported when $A_s = 0$

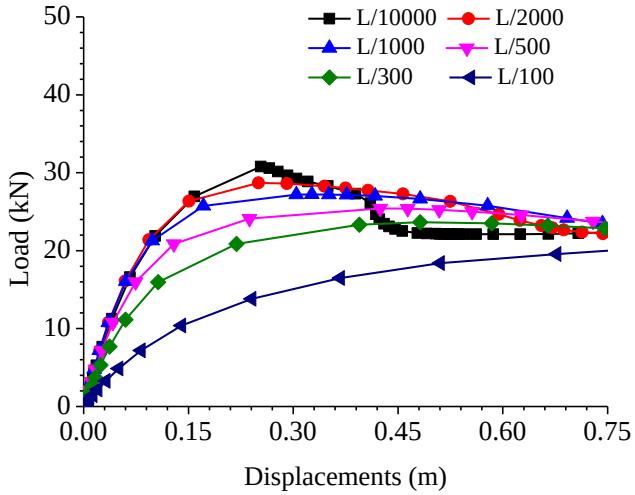

(e) Ini-pin supported when $A_s = 150$ mm^2

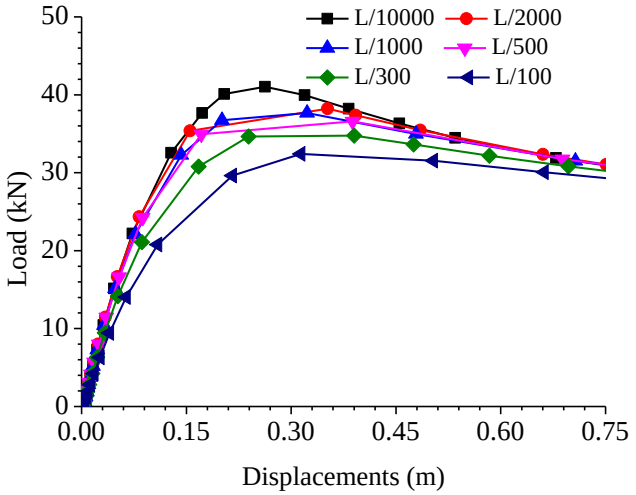

(f) Ini-fix supported when $A_s = 150$ mm^2

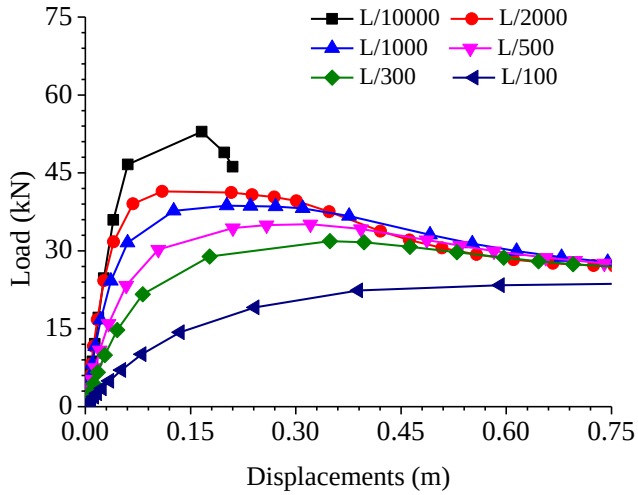

(g) Opt-pin supported when $A_s = 150$ mm^2

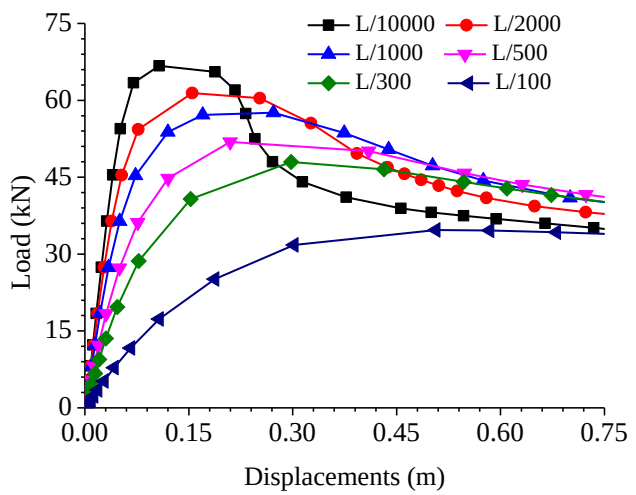

(h) Opt-fix supported when $A_s = 150$ mm^2

Fig. 17 Load versus displacement curves of USLS and CSLS with different imperfection magnitudes

It should also be noted that as the imperfection gets larger, the differences between the buckling resistances of initial and optimized shapes are gradually decreasing (the L/100 curve in Fig. 17(f) is reaching the same level of resistance as in Fig. 17(d)), indicating that the proposed shape optimization has limited contribution to the structural performance of latticed shells when they are subjected to very large imperfections.

Overall, the buckling analyses concluded that the USLS and CSLS are more imperfection sensitive after the proposed shape optimization, and as the imperfection gets larger, the benefit brought by optimization decreases. Therefore in design practice, realistic imperfection amplitudes must be taken into account.

6. Conclusions

In this study, a novel shape optimization method for single-layer two-way cable-stiffened latticed shells has been proposed. The method adopts a linear algorithm to minimize the strain energy of latticed shells with initial cylindrical profiles. Using this method, optimized shapes were achieved for a range of stiffened and unstiffened shells with varying cable sizes and under pinned and fixed boundary conditions. The structural responses (strain energy, critical buckling load, displacement, normal stress in members) have been compared for shells before and after optimization to investigate the efficiency of the proposed optimization method. Nonlinear buckling analyses considering geometric imperfections and material nonlinearities were also performed on the original and optimized shells. The main results can be summarized as follows:

- Compared to cylindrical shapes, the optimized shapes of two-way aluminum alloy single-layer latticed shells possess higher load-carrying capacities and improved structural performances. It is therefore possible for engineers to design aluminum alloy single-layer latticed shells with superior stability behaviors using this shape optimization method.
- The introduction of pre-tensioned cables in two-way aluminum alloy cylindrical latticed shells can significantly enhance the stability performance; however, the significance of this effect is also related to the boundary conditions, where the improvement is especially pronounced for shells with all the four edges fixed supported.

- The imperfection sensitivity study shows that imperfection deteriorates the load-carrying capacities of two-way aluminum alloy single-layer latticed shells, especially in fixed supported shells and cable stiffened shells. It is therefore suggested to take into account of realistic imperfection amplitude in design practice.

It should be noted that in this study the member connections of latticed shells were assumed to be fully rigid during the optimization and buckling analyses. However, the connections between the shell members in practice can be semi-rigid, and the optimization will become non-linear when the semi-rigid behavior is considered. It is therefore worth exploring a nonlinear shape optimization procedure in the future.

Acknowledgements

This research was supported by the National Natural Science Foundation of China (Nos. 51808070 and 51890902), the Fundamental and Frontier Research Project of Chongqing (No. cstc2018jcyjAX0535), the Fundamental Research Funds for the Central Universities (No. 2020CDJQY-A064), and Doctoral Research Fund of Shandong Jianzhu University (No. X19032Z). Their financial support is gratefully acknowledged.

References

[1] Li PC, Wadee MA, Yu JL, Christie NG, Wu ME. Stability of prestressed stayed steel columns with a three branch crossarm system. J Constr Steel Res, 2016, 122: 274-91.

[2] Schlaich J, Schober H. Glass Roof for the Hippo House at the Berlin Zoo. Struct Eng Int, 1997, 7(4):252-254.

[3] Wang H, Li PC, Wu ME. Crossarm length optimization and post-buckling analysis of prestressed stayed steel columns. Thin Wall Struct, 2019, 144: 106371.

[4] Li PC, Li ZQ, Jia B, Wang H. Stability analysis of prestressed stayed steel columns with split-up crossarm systems. Steel Compos Struct, 2020, 34(5): 769-782.

[5] Schlaich J, Schober H. Glass-covered Grid-Shells. Struct Eng Int, 1996, 6(2): 88-90.

[6] Feng RQ, Ye JH, Yao B. Evaluation of the Buckling Load of an Elliptic Paraboloid Cable-Braced

Grid Shell Using the Continuum Analogy. J Eng Mech. (ASCE), 2012, 138(2): 1468-1478.

[7] Kato S, Yamashita T. Evaluation of elasto-plastic buckling strength of two-way grid shells using continuum analogy. Int J Space Struct, 2002, 17(4): 249-261.

[8] Kato S, Yamashita T, Nakazawa S, Kim Y-b, Fujibayashi A. Analysis based evaluation for buckling loads of two-way elliptic paraboloidal single layer lattice domes. J Constr Steel Res, 2007, 63(9): 1219-1227.

[9] Li PC, Wu ME, Wang H, Shi MZ. Experimental and numerical analysis of cable-stiffened single-layer spherical latticed shell. Adv Struct Eng, 2016, 19(3): 488-499.

[10] Zhang Z, Fujimoto M. Effect of tension member on buckling and strength behavior of single layer two-way grid cylindrical shell roof. Journal of the International Association for Shell and Spatial Structures, Shanghai, 2010, 432-434.

[11] Li PC, Wu ME. Stabilities of cable-stiffened cylindrical single-layer latticed shells. Steel Compos Struct, 2017, 24(5): 591-602.

[12] Yamashita T, Kato S. Elastic buckling characteristics of two-way grid shells of single layer and its application in design to evaluate the non-linear behavior and ultimate strength. J Constr Steel Res, 2001, 57(12): 1289-1308.

[13] Fujimoto M, Kushima S, Imai K, et al. Numerical study on buckling behavior of single layer two-way grid dome with tension member as diagonals. Proceeding of the International Association for Shell and Spatial Structures (IASS) Symposium, Shanghai, 2010.

[14] Bulenda Th, Knippers J. Stability of grid shells. Comput Struct, 2001; 79(12): 1161-1174.

[15] Cedron F, Elghazouli AY. Seismic performance of single layer steel cylindrical lattice shells. J Constr Steel Res, 2019, 163: 105772.

[16] Ou Y, Luo YF, Huang QL, Zhu ZC. Seismic response evaluation of single-layer latticed shells based on equivalent modal stiffness and linearized iterative approach. Eng Struct, 2020, 204: 110068.

[17] Sasahara K, Hiep HT, Matsumoto Y. Evaluation method of seismic response by using mdof model and continuum shell analogy for single layer latticed cylindrical shell structures. J of Struct and Construct Eng, 2014, 79(705): 1647-1656.

[18] Ogawa T, Yamaoka K, Minowa K, Takeuchi T. Buckling strength of single layer lattice domes under static seismic load. J of Struct and Construct Eng, 2014, 79(704): 1523-1533.

[19] Alan H. The art of Structural Engineering. Stuttgart: Edition Axel Menges, 1997.

[20] Umezawa R, Hiraoka K, Takahashi H, et al. On design of Kumagaya Dome of a super large single layer reticular dome with membrane roof recently constructed in Japan. Proceedings of IASS-APCS 2003, Taipei, 2003.

[21] Ouyang YW, Qiu LQ, Li ZQ. Application and development review of large-span aluminum alloy structure. Build Struct, 2018, 48(14): 1-7. (in Chinese)

[22] Liu HB, Ding YZ, Chen ZH. Static stability behavior of aluminum alloy single-layer spherical latticed shell structure with Temcor joints. Thin Wall Struct, 2017; 120: 355-365.

[23] Xiong Z, Guo XN, Luo YF, Zhu SJ. Elasto-plastic stability of single-layer reticulated shells with aluminium alloy gusset joints. Thin Wall Struct, 2017; 115: 163-175.

[24] Ohsaki M, Ogawa T, Tateishi R. Shape optimization of curves and surfaces considering fairness metrics and elastic stiffness. Struct Multidiscip O, 2002, 24(6): 449-456.

[25] Firl M, Bletzinger KU. Shape optimization of thin walled structures governed by geometrically nonlinear mechanics. Comput Method Appl M, 2012, 237: 107-117.

[26] Feng R, Ge J. Shape optimization method of free-form cable-braced grid shells based on the translational surfaces technique. Int J Steel Struct, 2013, 13(3): 435-444.

[27] Cui C, Jiang B, Wang Y. Node shift method for stiffness-based optimization of single-layer reticulated shells. Journal of Zhejiang University SCIENCE A, 2014, 15(2): 97-107.

[28] Ikeya K, Shimoda M, Shi J. Multi-objective free-form optimization for shape and thickness of shell structures with composite materials. Compos Struct, 2016, 135: 262-275.

[29] Wang H, Wu M. Study on the Shape Optimization of Cable-Stiffened Single-Layer Latticed Shells. Int J Steel Struct, 2018, 18(3): 924-934.

[30] Wang H, Wu M. Global shape optimization of free-form cable-stiffened latticed shell based on local optimal solutions. Eng Struct, 2018, 168: 576-588.

[31] Shi MZ, Xiang P, Wu ME. Experimental investigation on bending and shear performance of two-way aluminum alloy gusset joints. Thin Wall Struct, 2018, 122: 124-136.